ACS OMEGA

http://pubs.acs.org/journal/acsodf

Article

Photophysical and Electrical Properties of Highly Luminescent 2/6-Triazolyl-Substituted Push−Pull Purines

Armands Sebris, Irina Novosjolova,* Kaspars Traskovskis,* Valdis Kokars, Natalija Tetervenoka, Aivars Vembris, and Māris Turks*

Cite This: *ACS Omega* 2022, 7, 5242−5253

Read Online

ACCESS | Metrics & More | Article Recommendations | Supporting Information

ABSTRACT: New push−pull *N*(9)-alkylated 6-piperidino-2-triazolylpurine and 2-piperidino-6-triazolylpurine derivatives are synthesized, and their optical and optoelectronic properties are comprehensively characterized with experimental and computational methods. The compounds possess intense violet or blue fluorescence with fluorescence quantum yields of up to 91% in solution and 40% in host-free films. Depending on their structural composition, the compounds have ionization energy in the range of 5.25−6.04 eV, electron affinity of 2.18−3.15 eV, and triplet energy of 2.52−2.95 eV. Due to the presence of hole-transporting purine and electron-transporting triazole fragments, compounds exhibit bipolar charge-transportation ability. Despite the favorable emissive properties of the studied push−pull purines, their electroluminescence in thin films is quenched owing to large current densities that are present even at a moderate driving voltage. This marks application directions related to a predominantly charge-transportation functionality as the most suitable for this compound class.

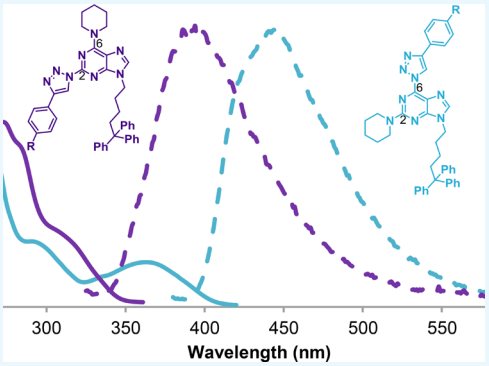

INTRODUCTION

DNA nucleobases have been successfully incorporated in electron-blocking or hole-transporting layers of organic light-emitting diodes (OLEDs) due to their large band gap (E_g) values and suitable energy levels.[1,2] Additionally, carbazole-functionalized DNA has been used as a charge-transporting co-host material in the active emissive layer (EML), consequently showing performance improvements in comparison to some conventional host materials.[3] Nucleobases or their derivatives have also been used in organic field-effect transistors (OFETs), mainly as the dielectrics.[4,5]

Recent studies have shown that chemical modifications of one of the nucleobase cores, the purine heterocycle, by an introduction of electron donor and acceptor fragments, provide highly emissive push−pull-type compounds, whose fluorescence (FL) quantum yield (Φ_{FL}) can reach unity.[6−11] While the fluorescent nature of these compounds limits the potentially attainable efficiency of the corresponding purine-based OLEDs, singlet harvesting compounds still find a practical use in blue light-emitting devices due to the poor chemical stability of the triplet harvesting alternatives.[12] Several early reports of OLEDs showing electroluminescence in the important deep-blue and violet parts of the spectrum have been demonstrated using purine-based emitters.[13,14] In addition, it was recently reported that 9-methylpurine-based derivatives containing phenoxazine groups in the para-position of the phenyl substituent at C6 or C2 and C6 positions of purine possess thermally activated delayed fluorescence, further underlining the potential prospects of the compound class for the application in organic electronic devices.[15] On the other hand, purine derivatives containing phenoxazine or phenothiazine groups in the meta-position of the phenyl substituent synthesized by us reached only up to 15% quantum yields in PMMA-based films.[16]

In 2021, we designed TADF-active exciplexes based on 6-cyano-9-phenylpurine-carbazole dyads, studied their photophysical properties in the solution, film, and crystalline phase and successfully used them as host materials for the emissive layer in OLEDs.[17] In this paper, we investigate the practical application feasibility and possible limitations of fluorescent push−pull purines containing triazolyl moieties, focusing on the compound integration in solution-processed films with electroluminescent or charge-transporting functionality and studying the optical and optoelectronic properties of synthesized purine derivatives. A series of *N*(9)-alkylated 6(or 2)-piperidino-2(or 6)-triazolylpurine push−pull-type molecules were acquired for the purpose of the study. The photophysical and thermal properties of the compounds and their energy level configuration were experimentally determined. The experimental data were supplemented with quantum-chemical calculations. The

Received: November 11, 2021
Accepted: January 13, 2022
Published: February 2, 2022

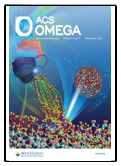

https://doi.org/10.1021/acsomega.1c06359
ACS Omega 2022, 7, 5242−5253

Scheme 1. General Synthetic Routes for the Synthesis of Triazolylpurines 5a−d and 9a−d

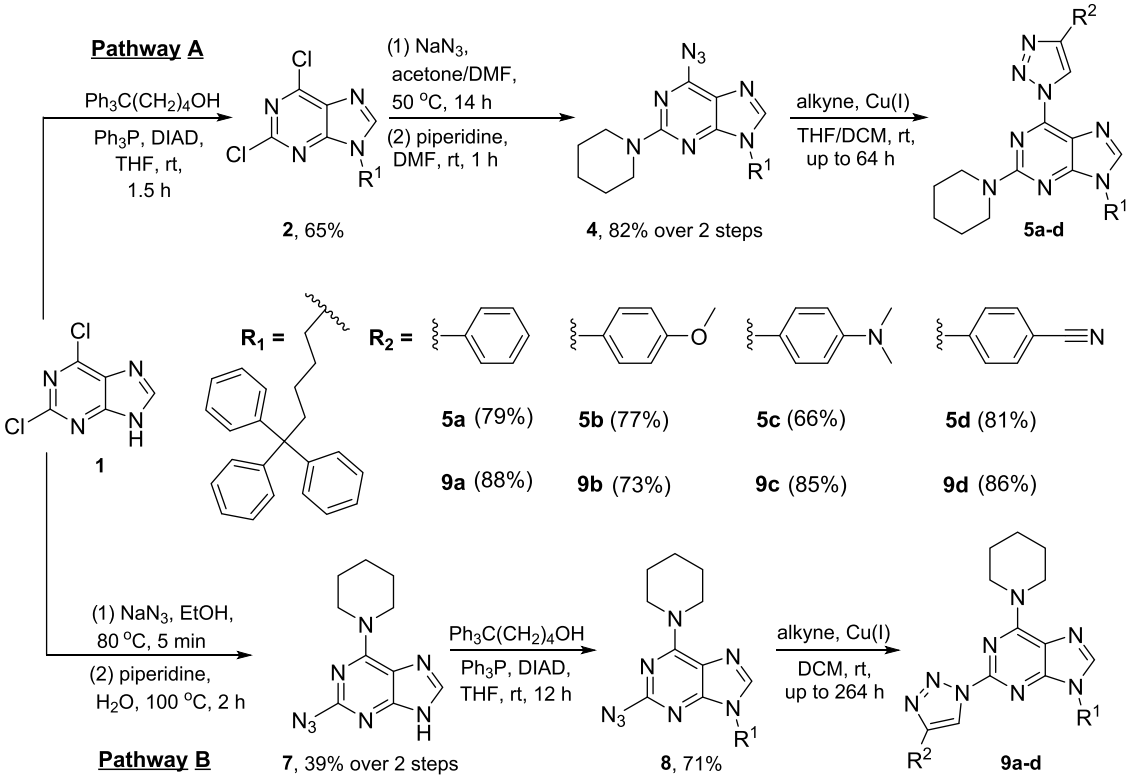

results indicate that the compounds exhibit excellent charge-transporting ability, which is detrimental to the electroluminescence process but can be potentially exploited in purely charge-transportation-related areas of organic electronics.

RESULTS AND DISCUSSION

Material Design and Synthesis. The newly synthesized materials were based on a known highly emissive molecular scaffold,[18−23] where 2- or 6-amino-substituted purines are functionalized with electron-deficient 1,2,3-triazole moieties at the corresponding unoccupied 2- or 6-position. It has been shown that natural 2- or 6-amino-substituted purine derivatives, guanine and adenine, possess good hole-transporting ability.[1] The presence of 1,2,3-triazole moieties, on the other hand, is shown to enhance the electron transport properties of the molecule.[24] It was predicted that the suggested bipolar composition of the target molecules would facilitate balanced charge-transporting properties. To better understand correlations between the structure and photophysical properties of the compounds, differently substituted phenyl groups were attached to the triazole cycle. The poor solubility and inherent crystallinity of the corresponding purine derivatives were overcome with the introduction of 5,5,5-triphenylpentyl groups. Triphenylmethane-based derivatives are known to promote amorphous phase formation for otherwise crystalline polar molecules.[25]

For the synthesis of the desired compounds, we used two different approaches (Pathway A and B), yielding compound series **5a−d** and **9a−d** (Scheme 1). The commercially available 2,6-dichloropurine **1** was used as the starting material. For the synthesis of compound **5**, first, we introduced a triphenylpentyl group at the *N*(9) position of purine using DIAD, Ph_3P, and corresponding alcohol under the Mitsunobu conditions.[26,27] Then, we substituted chlorine atoms at C(2) and C(6) positions with azido groups and next introduced piperidine as a donating group. For *N*(9)-alkylated substrates, substitution with piperidine took place at the C(2) position and subsequently the triazolyl ring was introduced at the C(6) position via Cu(I)-catalyzed cycloaddition reactions with different alkynes. Previously reported methods have been used for the copper-(I)-catalyzed alkyne-azide cycloaddition (CuAAC) reactions to produce triazole moieties.[19,28] Products **5a−d** were obtained with 66−81% yields (Scheme 1).

On the other hand, series **9** were obtained using the same reaction conditions but in a reverse sequence (Scheme 1). First, unprotected 2,6-dichloropurine **1** was treated with NaN_3 followed by an S_NAr reaction with piperidine. In the case of *N*(9)-H 2,6-diazidopurine, the S_NAr reaction with piperidine took place regioselectively at the C(6) position, which is opposite to *N*(9)-alkylated substrates. Next, product **7** was alkylated at the *N*(9) position and products **8** were cyclized with different alkynes to target products **9a−d**. These 1,3-dipolar cycloaddition reactions required longer times compared to previous ones but still produced products **9a−d** with 73−88% yields. For example, a reaction with 4-dimethylaminophenylacetylene required 264 hours to be completed. An increase of the temperature to accelerate the cycloaddition was impossible due to the instability of azido starting materials. Moreover, all of the steps, where the azido group was involved, were performed while being covered from the day light. All azido compounds (**4**, **7**, **8**) should be stored at temperature ≤ -20 °C to prevent degradation.

Phase Behavior and Thermal Characteristics. With the introduction of triphenylpentyl groups that enhance solubility and promote the formation of an amorphous phase, the synthesized compounds were primarily designed as being suitable for solution-based processing methods. The resulting purine derivatives are highly soluble in moderate polarity

https://doi.org/10.1021/acsomega.1c06359
ACS Omega 2022, 7, 5242−5253

solvents ($CHCl_3$, DCM, THF) and form amorphous films upon spin-coating from the corresponding solutions. To closely investigate the solid-state phase behavior, the selected compounds **5a**, **5d**, **9a**, **9b**, and **9d** were studied by employing differential scanning calorimetry (DSC). From this series, only compound **9d** showed the presence of a crystalline state upon the first heating cycle (melting temperature 176.0 °C). In the case of other compounds, glass transition temperature (T_g) was detected as the only phase transition. DSC plots of the second heating cycle for the purine derivatives are given in Figure 1. The

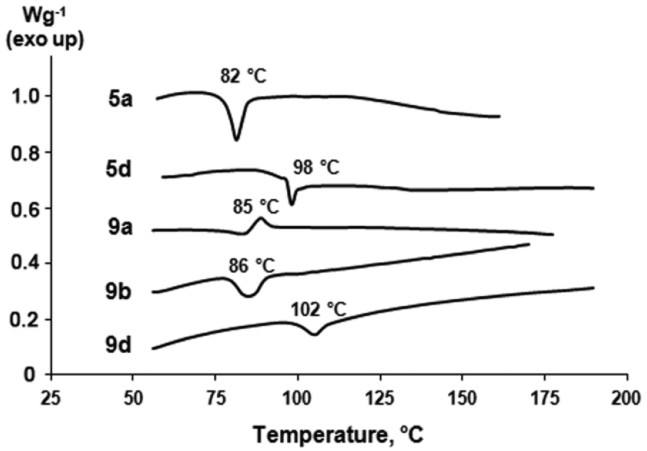

Figure 1. DSC plots during the second heating for selected push−pull purine derivatives.

obtained T_g values vary in the range of 82−102 °C. These parameters are sufficient to ensure the structural integrity and to prevent phase transition processes in optoelectronic devices under typical device operation conditions. For comparison, T_g of a conventional charge-transporting host material as 4,4′-bis(*N*-carbazolyl)-1,1′-biphenyl (CBP) is 62 °C.[29] Structural correlations among the series of the synthesized compounds reveal that T_g increase in the range of 13−20 °C can be linked with the presence of the cyanophenyl group (compounds **5d**, **9d**). As it is indicated by DFT calculations, which evaluate the ground state dipole moment (μ) values of **5d** and **9d** at μ = 11.9 and 10.5 D (Table S1), these molecules are the most polar among the examined series. Further discussion concerning molecular orbital placement relates this to an increased spatial separation of electron-rich and poor regions of the molecules. Since μ can be associated with a strong amplification in the force of solid-state intermolecular interactions,[30] the consequential rigidification of the glassy lattice manifests in increased T_g for **5d** and **9d**. The same explanation can be given for the outlier crystallization tendency for compound **9d**, which is also caused by the high polarity of the compound.

The presence of *N*-heterocyclic molecular fragments has often been linked to a reduced thermal and chemical stability of the corresponding molecules.[31,32] Thermogravimetric analysis was performed to evaluate the thermal stability of the compounds **5d** and **9d** (Figure S1). The results show that both the molecules possess good thermal stability with the corresponding decomposition temperatures of 298 and 258 °C. A notable increase in stability can be observed for a purine derivative with a 2-amino-6-triazolyl substitution pattern in comparison to a 2-triazolyl-6-amino counterpart.

Photophysical Characterization. The synthesized materials were initially characterized employing UV−vis absorption and photoluminescence (PL) spectroscopy. The obtained absorption and emission bands are given in Figure 2, and band maxima values are outlined in Table 1. Taking into account the structural impact on the photophysical properties, the placement of substituents at the purine ring in either 2-amino-6-triazolyl (series **5**) or 2-triazolyl-6-amino (series **9**) arrangement has the most notable impact on electronic transitions. In the case of **5**, UV−vis absorption spectra feature intense bands in the 250−300 nm range that can be attributed predominantly to the local excitation (LE) of the purine aromatic system.[33,34] The lowest energy bands with maxima at 360−367 nm, on the other hand, correspond to intramolecular charge-transfer (ICT) transitions. The FL spectra of **5** exhibit wide featureless emission bands in the blue spectral region (maxima at 439−448 nm). Considering the aromatic substituents at the 1,2,3-triazole ring, only the introduction of *N*,*N*-dimethylaniline (**5c**) causes a notable deviation in emissive properties, redshifting the FL band by approximately 60 nm. We relate this observation to a stronger solvatochromic response of the compound and the resulting stabilization of the excited state energy level. This is presumably caused by the presence of nitrogen lone pair, which may enhance specific solute−solvent interactions, such as hydrogen bonding.[35] Because of this, dialkyl substituted amines are common structural fragments met in strongly solvatochromic dyes.[36] Φ_{FL} values for **5** vary in the range of 0.74−0.91 in solution. Generally, the introduction of electron-donating groups at 1,2,3-triazole can be associated with reduced Φ_{FL}. In spin-coated amorphous films, the compounds retain fairly large emission efficiency (Φ_{FL} = 0.40−0.28), indicating a moderate extent of solid-state quenching,[37,38] with the exception of **5c**, which shows a dramatic emission efficiency drop to 0.03.

For the 2-triazolyl-6-amino purine series (**9a**−**d**), the lowest energy absorption and FL bands show a substantial hypsochromic shift in comparison to the structural analogues from the 6-triazolyl-2-amino purine series (**5a**−**d**). ICT absorption bands ($\lambda_{abs\ max}$ 300−305 nm) now partly overlap with LE transitions, while emission has shifted to the violet part of the spectrum ($\lambda_{em\ max}$ 388−455 nm). Analogous to the previously observed behavior, only the introduction of the *N*,*N*-dimethylaniline fragment to the 1,2,3-triazole moiety causes a notable redshift of absorption and FL bands. Φ_{FL} values in solution for **9a**−**d** (0.17−0.44) are notably lower than those measured for **5**. On the other hand, in amorphous films, series **9** show a relatively lesser FL efficiency drop (0.15−0.22), with the exception of *N*,*N*-dimethylaniline-substituted **9c**.

All compounds show monoexponential emission decay curves, associable with a fluorescence process (Figure S2). Lifetime values vary in the range of 11−13 ns for series **5**, while for compounds **9**, the emissive relaxation to the ground state proceeds substantially faster, in the range of 2−8 ns (Table 1). The corresponding radiative (k_r) and nonradiative (k_{nr}) decay rates (Table S2) indicate that k_r is somewhat comparable among all compounds, but k_{nr} is notably increased for series **9**. It is worth noting that the FL lifetime of the compounds is longer than typical values for purine-based emitters.[6] As shown by Collier et al., the emission rate in such emitters decreases as the π-conjugation system of the emitter expands and the charge-transfer process is not confined to the purine moiety but assumes an intramolecular charge-transfer character.[9] A similar situation is observed for our compounds, where the emissive process involves charge transfer between different aromatic fragments.

All of the studied compounds show a positive solvatochromic response for FL bands, without notable band shape trans-

https://doi.org/10.1021/acsomega.1c06359
ACS Omega 2022, 7, 5242−5253

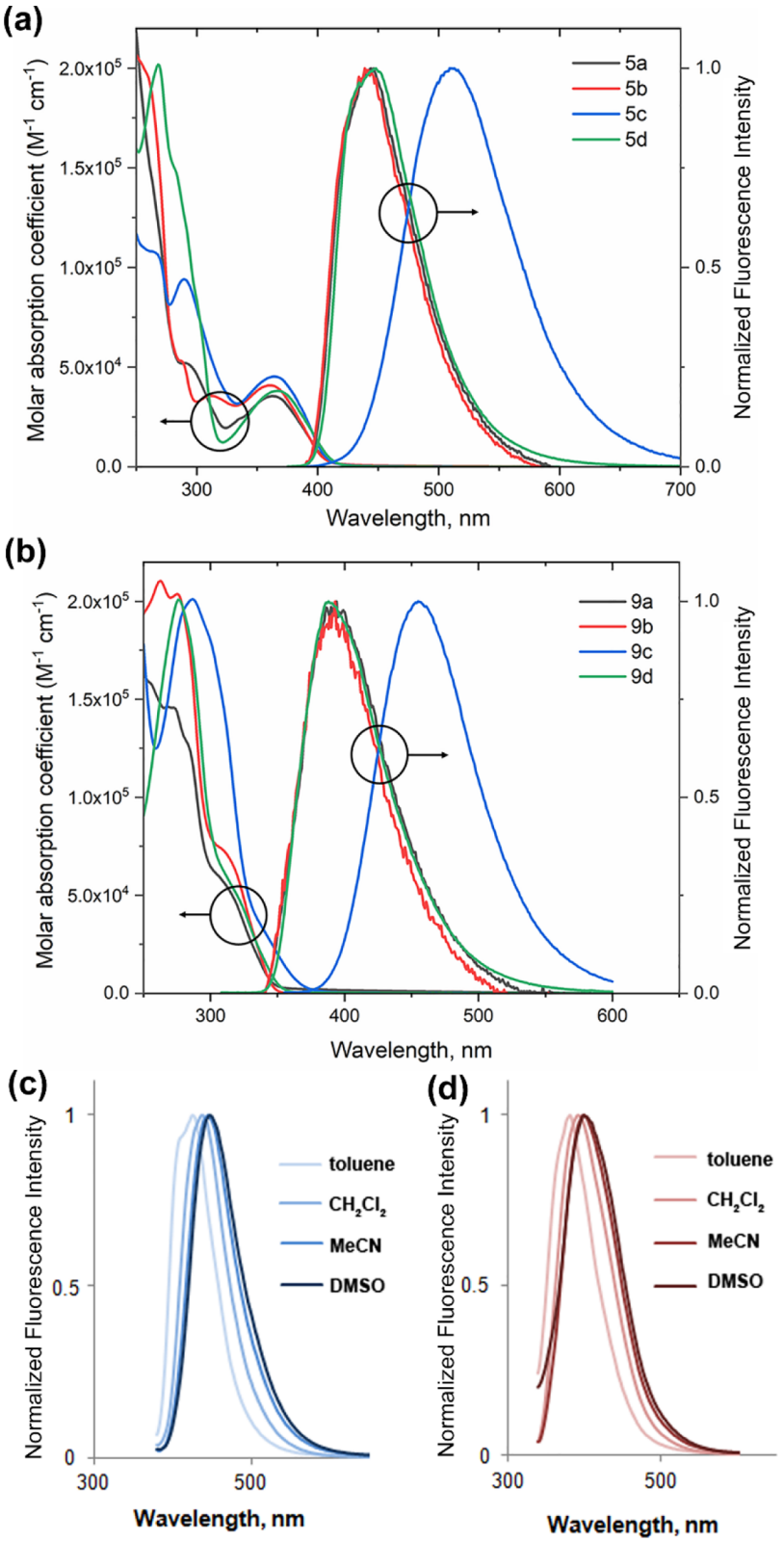

Figure 2. Absorption and emission spectra for compound series **5** (a) and **9** (b) measured in CH_2Cl_2. Solvatochromic response for emission bands of **5a** (c) and **9a** (d).

formations (see Figure 2c,d for the solvatochromic response of **5a** and **9a**). This indicates a dipole moment increase of the molecules upon the excitation process and points to the ICT character of the excited states.[36]

Characterization of Electronic Levels. The configuration of electronic levels for optoelectronic materials determines whether compounds are compatible with an incorporated emitter, host material, or neighboring layers of the charge-transporting materials or electrodes. The electronic levels in thin

https://doi.org/10.1021/acsomega.1c06359
ACS Omega 2022, 7, 5242−5253

Table 1. Experimental and Calculated Photophysical Parameters and Energy Levels for Compounds 5a−5d and 9a−9d

	experimental								calculations			
compound	$\lambda_{abs.ma}$, nm[a]	$\lambda_{em.\ max}$, nm[a]	Φ_{PL}[b]	τ, ns[a]	E_T, eV[c]	I_E, eV[d]	A_E, eV[e]	E_{th}, eV[f]	HOMO, eV	LUMO, eV	ΔE_{S0-S1}, eV[g]	ΔE_{S0-T1}, eV[h]
5a	364	446	0.91/0.32	13	2.53	5.80	2.85	2.95	−5.61	−1.63	3.57	2.75
5b	360	439	0.78/0.28	11	2.54	5.86	3.07	2.79	−5.45	−1.56	3.51	2.76
5c	365	511	0.74/0.03	12	2.52	5.25	2.47	2.78	−4.86	−1.45	3.06	2.61
5d	367	448	0.90/0.40	12	2.54	5.90	3.15	2.75	−5.79	−1.96	3.42	2.69
9a	320	394	0.31/0.22	3.6	2.93	5.76	2.31	3.45	−5.73	−1.23	4.09	3.19
9b	320	399	0.17/0.15	2.0	2.95	5.85	2.59	3.26	−5.41	−1.16	3.87	3.08
9c	330	455	0.30/0.03	7.9	2.75	5.25	2.18	3.07	−4.86	−1.05	3.44	2.88
9d	330	388	0.44/0.20	3.9	2.87	6.04	2.89	3.15	−5.99	−1.75	3.81	3.08

[a]Measured in CH_2Cl_2. [b]Values in CH_2Cl_2 solution and films. [c]Triplet energy levels, determined in 2-MeTHF at 77 K. [d]I_E − ionization energy. [e]A_E − affinity energy. [f]E_{th} − photoconductivity threshold value. [g]Calculated lowest singlet excitation energy. [h]Calculated lowest triplet excitation energy.

spin-coated amorphous films of the synthesized compounds were determined by photoemission yield spectroscopy, to find ionization energy (I_E), and photoconductivity measurements, to determine the photoconductivity threshold value (E_{th}). The electron affinity level (E_A) was then calculated as the difference between I_E and E_{th}. The obtained values are outlined in Table 1. In agreement with the previously discussed results of photophysical characterization, the electronic level measurements confirm a clear distinction between compounds **5** and **9**. E_{th} of **5** (2.75−2.95 eV) are lower than for **9** (3.07−3.45 eV), indicating notably higher band gap values for the latter series of compounds. Several structure−property relationships can be observed. First, among the structurally comparable compound pairs that contain identical aryl substituents at the 1,2,3-triazole ring, the I_E value is almost not influenced by the attachment pattern of amino and triazole substituents at the purine ring. This energy level is only affected by the substituents at the 1,2,3-triazole-attached phenyl ring. The A_E level placement, on the other hand, is affected by both these structural variations. In general, the introduction of the *N*,*N*-dimethylaminophenyl fragment at 1,2,3-triazole causes destabilization of I_E and A_E levels. This could be explained by the resulting donor−acceptor−donor (D−A−D) type configuration of the resulting conjugated molecules that reduce delocalization energy of the push−pull system. In contrast, the presence of the electron-deficient cyanophenyl group causes stabilization of I_E and A_E, as the molecules form an extended D−A system now. The compounds that contain an electronically neutral phenyl group show the largest E_{th} values, as the lack of electron-accepting or -donating groups reduces their overall push−pull character.

The determination of triplet energy levels (E_T) is crucial for host materials that are being designed for triplet harvesting emitters. If E_T of the charge-transporting material is higher than that for the emissive compound, exothermic excited triplet state migration proceeds to the emitter. If the situation is reversed, the triplet states largely stay on the host molecules, negatively affecting the corresponding OLED efficiency.[39] E_T of the synthesized compounds was determined by employing low-temperature phosphorescence measurements in a frozen 2-methyltetrahydrofuran matrix at 77 K. Triplet energies were assigned at the highest energy phosphorescence band maxima (see Figures 3 and S3). For series **5**, E_T values vary in the range of 2.52−2.54 eV (Table 1), but for **9a**, **b**, **d**, they are 2.87−2.95 eV, with **9c** being an outlier at 2.75 eV. These values suggest that compounds **9** can be potentially used as host materials for blue-phosphorescent compounds.

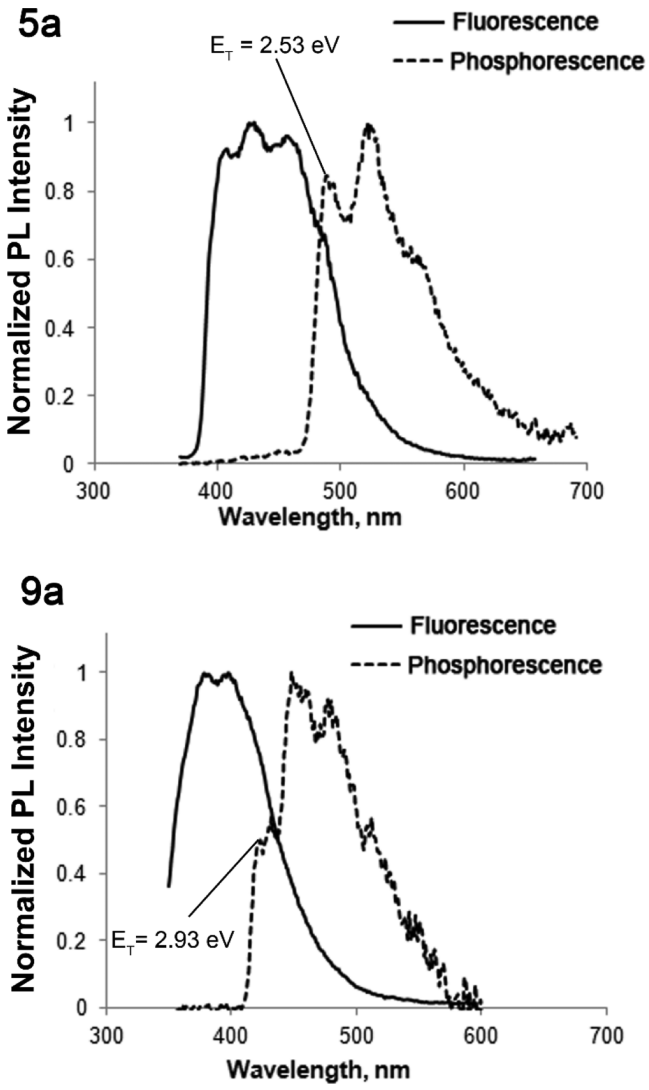

Figure 3. Fluorescence and phosphorescence spectra of **5a** and **9a** in the 2-MeTHF matrix at 77 K.

Quantum-Chemical Calculations. DFT calculations for the synthesized compounds were performed to better explain the correlations between the synthesized structures and their photophysical properties. The numerical values of the highest occupied molecular orbital (HOMO), lowest unoccupied molecular orbital (LUMO) energy levels, and singlet and triplet excitation energies are outlined in Table 1, but the visualizations

https://doi.org/10.1021/acsomega.1c06359
ACS Omega 2022, 7, 5242−5253

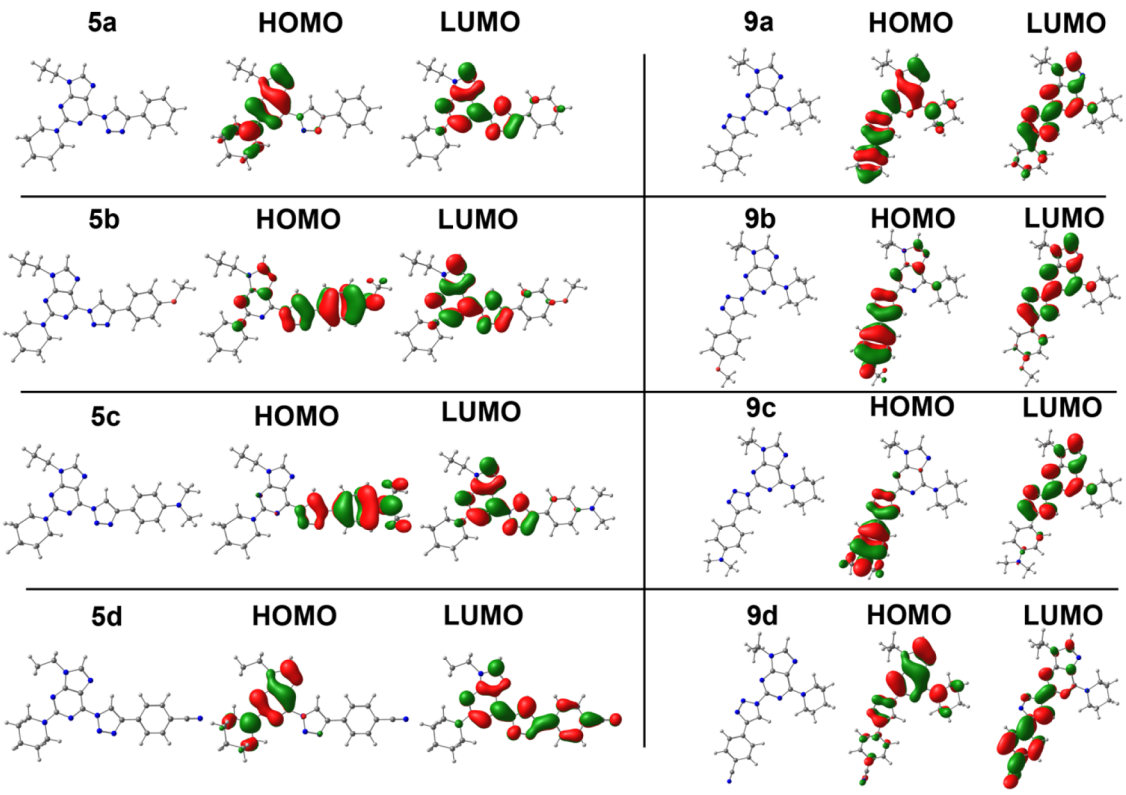

Figure 4. Calculated geometries and HOMO/LUMO distribution for compounds **5a−d** and **9a−d**.

of the orbitals are given in Figure 4. The optimized structures of the compounds assume conformations, where all of the present aromatic ring systems are coplanar, indicating that π-electrons are delocalized in a conjugated system and no sterical overcrowding effects take place that would result in a twisted geometry. Generally, a good agreement between the experimental and DFT values can be found, as the calculated HOMO and LUMO energy level values correlate well with the measured ionization potentials and electron affinities.

As it can be concluded from the previously discussed experimental results, regarding the substitution pattern at 2- and 6-positions, the photophysical and electronic characteristics of the compounds change drastically. This discrepancy between **5** and **9** is partly explained by the molecular orbital configuration of the compounds. In the case of **5a**, purine-centered HOMO and triazole-centered LUMO are much more spatially separated than for **9a**, where these frontal orbitals are delocalized all over the conjugated ring system and largely overlap. This points to a more pronounced push−pull characteristic for **5a** and its analogues. The assumption is additionally supported by the calculated band gap values that show a substantial drop in $\Delta E_{\mathrm{HOMO-LUMO}}$ for **5** in comparison to **9**. The differing nature of the molecular orbital configuration may also explain the detected drastic variations in nonradiative excitation decay rates (k_{nr}) between the two compound subsets. The less contained molecular orbitals for series **9** compounds would result in the excited states that are delocalized across multiple aromatic ring systems, thus increasing the susceptibility to relaxation pathways through vibrational or conformational motion processes.

The introduction of electron-donating groups at the 1,2,3-triazole fragment drastically changes the molecular orbital configuration for the compounds, as HOMO then localizes on the corresponding electron-rich aryltriazole moiety, while LUMO is mostly confined to the purine fragment. Despite this transformation of the electronic system, in terms of molecular orbital energy values, this causes no major deviations in regard to other synthesized compounds. For **5d** and **9d**, the presence of the electron-accepting cyanophenyl group enhances the spatial separation between the purine-centered HOMO and the triazole-based LUMO by shifting the LUMO to the corresponding electron-deficient benzene ring and the cyano group. Such increased push−pull characteristic is considered as the origin for the experimentally observed stabilization of I_{E} and A_{E} levels in comparison to the rest of the synthesized compounds. This also reflects in the increased calculated ground state dipole moment values of the compounds.

Optoelectronic Properties. The evaluation of the synthesized compounds for use in optoelectronic devices was initially carried out by the preparation of OLEDs, where solution-processed EMLs consisted only of the synthesized purine derivatives. Purines with the highest fluorescence quantum yield were chosen for OLED preparation, namely, **5a**, **5d**, **9a**, and **9d**. In all of the cases, no electroluminescence originating from purine derivatives was observed. At the same time, the prepared OLEDs showed relatively large current densities, as the values exceeding 100 mA/cm^2 were measured at a driving voltage of 5−7 V (Figure S4). High current can be proposed as the main reason for the lack of detectable emission. Polaron concentration in EML at such current levels is high and, most likely, an extensive polaron-exciton quenching takes place. In addition, high current promotes a current leakage. The prevalence of nonradiative exciton recombination pathways under such conditions results in excessive heating that can further reduce the performance parameters of light-emitting diodes.[40] An unbalanced charge carrier injection in the devices

https://doi.org/10.1021/acsomega.1c06359
ACS Omega 2022, 7, 5242−5253

was proposed as another possible cause for the lack of measurable emission.

After unsuccessful attempts to use the purines as the emitting compounds, these compounds were tested as potential charge-transporting host materials for phosphorescent triplet emitters. Based on its highest measured triplet energy value, compound **9b** was chosen as the most suitable material for such a purpose. Tentative OLEDs with EML composed of conventional iridium(III) blue emitter FIrpic (10 wt %) and **9b** were prepared. Unfortunately, an identical result as in purine-only samples was obtained since devices exhibited no electroluminescence. To better understand the possible cause for this poor OLED performance, a multi-host device with ITO/PEDOT:PSS/EML/BPhen/LiF/Al architecture was prepared, where EML consisted of FIrpic/**9b**/CBP (10:30:60 wt %) (Figure 5). In this case, a measurable amount of luminance was

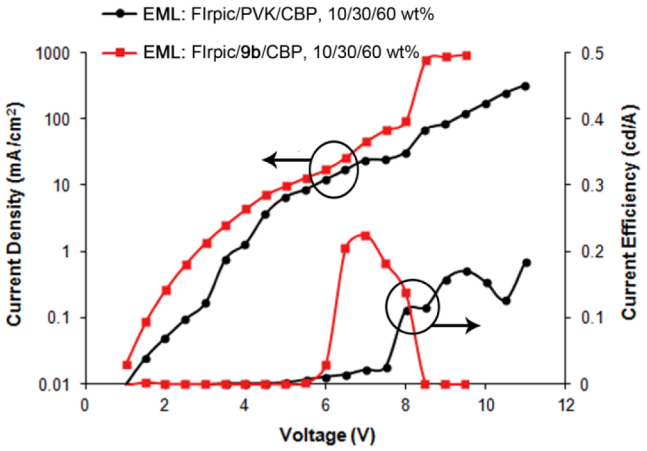

Figure 5. Current density and current efficiency-voltage dependencies for multi-host OLEDs.

detected, originating from the phosphorescent host. In comparison with a reference device with FIrpic/PVK/CBP (10:30:60 wt %) EML, the purine bearing OLED showed a notable increase in current density, indicating improved charge transport properties. The device also showed improved efficiency parameters at the voltage range slightly above the luminance onset mark. The further driving voltage increase, however, resulted in a sharp decrease in luminance, while the reference device experienced a steady rise in current efficiency. Such behavior indicates a better charge carrier density and balance at turn-on voltage levels in a purine-containing device, but a further voltage increase causes a rapid deterioration in the operational stability. Two possible reasons could be mentioned for the steep OLED efficiency decrease. Although better-balanced charge carries in the system, there is still high leaked current (around 10 mA/cm^2 at turn-on voltage) so that exciton quenching by polarons takes place at higher driving voltages. Second, the prepared emitter layer consists of only small molecules that could lead to higher FIrpic emitter aggregation compared to the system with an added polymer host (PVK). Consequently, exciton−exciton annihilation will be observed and will result in efficiency roll-off. The roll-off could be decreased by optimizing the ratio between **9b** and CBP. At a voltage of 8 V, a partial current shortage was observed that destroyed the OLED and no electroluminescence was observed.

Finally, single charge carrier devices were prepared using architectures ITO/LiF/purine **5d** or **9d**/LiF/Al for electron-only or ITO/MoO_3/purine **5d** or **9d** /MoO_3/Cu for hole-only transport measurement purposes (Figure 6). The obtained

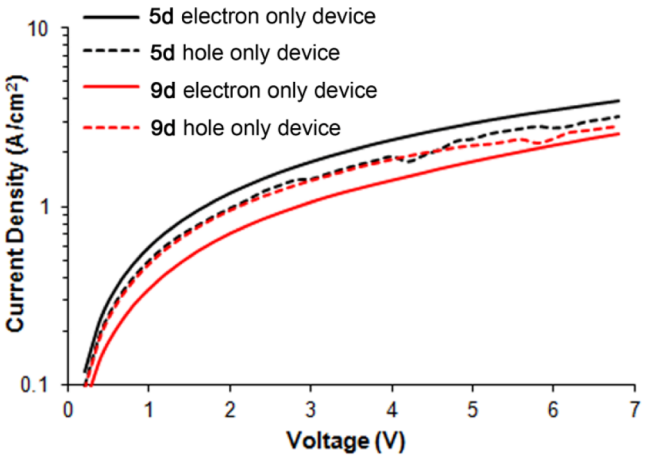

Figure 6. Current density−voltage characteristics for electron-only and hole-only devices of **5d** and **9d**.

results indicate that the compounds possess bipolar charge-transporting properties, as the hole and electron-only devices have similar voltage−charge density dependencies. At the same time, both compounds show very high current levels. Even at voltages as low as 2 V, the current density exceeds 1 A/cm^2 and this parameter reaches the 3 A/cm^2 mark with a voltage increase to 7 V. These current density values are more than an order of magnitude greater than those measured for readily applied OLED charge-transporting host materials.[41,42] This result confirms that the large current density in EML is the main reason for the poor OLED performance of the studied push−pull purines. The good charge-transporting ability of the acquired triazolyl functionalized purines can be attributed to their planar geometry and dipolar nature. Our previous investigation of closely similar structures has revealed that in the crystalline state these compounds tend to form highly ordered vertical stacks that are determined by dipolar $\pi-\pi$ interactions between the electron-rich purine and electron-deficient triazolyl ring systems.[43] Taking into account the good charge-transporting ability of the synthesized push−pull purines, their use as semiconductors in organic field-effect transistors (OFETs) or other devices with purely charge-transporting functionality can be proposed as the most promising application directions.

Interestingly, slight variations can be observed between charge transport properties for 2-amino-6-triazolyl (**5d**) and 2-triazolyl-6-amino (**9d**) configured compounds. While both compounds show almost overlapping current density−voltage dependency in the hole-only mode, **5d** exhibits vaguely better electron transportation ability. At the same time, **9d** is more prone to hole transport. The calculated distribution of frontier molecular orbitals for the corresponding compounds (Figure 4) shows that the HOMO in both cases similarly lies on the purine ring system, explaining the almost identical hole-transporting properties. The LUMO, on the other hand, is located mainly on the cyanophenyl ring for **9d** but is delocalized over the whole purine−triazole−phenyl system for **5d**. Increased LUMO delocalization seems to be beneficial for the overall electron-transporting ability of the push−pull purines.

https://doi.org/10.1021/acsomega.1c06359
ACS Omega 2022, 7, 5242−5253

CONCLUSIONS

The optical and optoelectronic properties of push−pull *N*(9)-alkylated 6-piperidino-2-triazolylpurine and 2-piperidino-6-triazolylpurine derivatives have been investigated. The interchangeable 2/6-substitution pattern of the studied compounds provides a molecular platform in which frontier molecular orbital energy levels can be greatly modified. This allows obtaining molecules with ionization energy in the range of 5.25−6.04 eV, electron affinity of 2.18−3.15 eV, and triplet energy of 2.52−2.95 eV. The compounds also exhibit strong fluorescence in violet and blue spectral regions, with the measured Φ_{FL} in solutions reaching 0.91. The functionalization of purines with phase modifying groups prevents crystallization of compounds and reduces solid-state emission quenching, allowing the preparation of amorphous spin-coated host-free films with Φ_{FL} of up to 0.40. While the emissive properties and high triplet energy levels could mark the synthesized compounds as promising candidates for either emitter or host materials in the emissive layers of OLEDs, no electroluminescence was observed in the corresponding devices. This can be attributed to an excessive charge-transporting ability of the compounds that leads to either current leakage or strong emission quenching due to the large current density in the emissive layer. On the other hand, the bipolar character and good charge-transporting ability of the investigated compounds can potentially be exploited to provide materials in other areas of organic electronics, such as organic field-effect transistors.

EXPERIMENTAL PART

General Information. ^{1}H- and ^{13}C-NMR spectra were recorded on Bruker Avance at 300 and 75.5 MHz, respectively. The proton signals for residual nondeuterated solvents (δ 7.26 for $CDCl_3$, δ 2.50 for DMSO-d_6) and carbon signals (δ 77.1 for $CDCl_3$, δ 39.5 for DMSO-d_6) were used as an internal reference for ^{1}H- and ^{13}C-NMR spectra, respectively.

Analytical thin-layer chromatography (TLC) was performed on Merck 60 Å silica gel F_{254} plates. Column chromatography was performed on Merck 40−60 μm 60 Å silica gel. Anhydrous methylene chloride, dimethylformamide, and acetonitrile were obtained by distillation over CaH_2, tetrahydrofuran was obtained by distillation over sodium. Commercial reagents were used as received. The infrared spectra were recorded on Perkin Elmer Spectrum BX. Wavelengths are given in cm^{-1}. For HPLC analysis, we used *A*gilent Technologies 1200 Series chromatograph equipped with an Agilent XDB-C18 (4.6 × 50 mm, 1.8 μm) column and a Phenomenex Gemini NX (4.6 × 100 mm, 3 μm) column. Eluent A: 0.01 M KH_2PO_4 solution with 6% v/v MeCN added; eluent B: 0.1% TFA solution with 5% v/v MeCN added; and eluent C: MeCN.

Optical measurements of solutions were carried out at a typical material concentration of 1×10^{-5} mol L^{-1}. The UV−vis absorption spectra were recorded with a Perkin Elmer Lambda 35 spectrometer. Films for optical measurements were prepared using a spin-coating technique with a Laurell WS-400B-6NPP/LITE spin-coater on glass slides, using $CHCl_3$ solutions with a material concentration of 30 mg/mL. After the preparation, all films were dried in an oven at 100 °C for 2 h. Emission spectra, Φ_{FL}, and lifetime values in solutions or thin films were measured using a QuantaMaster 40 steady-state spectrofluorometer (Photon Technology International, Inc.) equipped with a 6-inch integrating sphere by LabSphere, using the software package provided by the manufacturer. For lifetime measurements, excitation at 365 nm was used, while emission was detected at the respective band maxima. Low-temperature emission measurements were carried out by cooling the cuvettes in a liquid nitrogen-filled quartz Dewar. Phosphorescence spectra were recorded using time-gated detection by collecting emission in a 50−5000 μs interval after the excitation. Differential scanning calorimetry (DSC) thermograms were acquired using a Mettler Toledo DSC-1/200W apparatus. The samples were heated from 50 to 190 °C at a rate of 10 °C min^{-1} and isothermally aged for 5 min, then cooled to 50 °C at a rate of 10 °C min^{-1} and isothermally aged for 5 min. The cycle was repeated 3 times. Decomposition temperatures were obtained using a Perkin Elmer STA 6000 thermal analyzer.

The molecular ionization energy in a thin film (I_E) and photoconductivity measurements (E_{th}) were carried out on a self-made experimental system using a method described in our previous work.[44] The values of electron affinity energies in thin film (A_E) were calculated using the difference of experimentally determined values of E_{th} and I_E.

Density functional theory (DFT) calculations were performed using the ORCA[45] program package. For auxiliary tasks, the Avogadro program[46] was used. The geometry optimizations for all compounds were obtained using nonlocal functional B3LYP with a 6-311G**[47] basis set. Ground state dipole moment (μ) values were calculated at the same theory level. Initial atomic coordinates were chosen based on X-ray analysis data of closely related structures.[43] For TDDFT calculations, def2-TZVP basis, def2/J auxiliary basis, and the RIJCOSX approximation were used. To reduce the computational cost, the structures were simplified by substituting triphenylpentyl moieties with ethyl groups.

Sandwich-type samples with the pixel size of 16 mm^2 were prepared for the OLED, electron-only, and hole-only devices. Indium tin oxide (ITO) glass (Präzisions Glas & Optik GmbH) with a sheet resistivity of 50 Ω^2 was used as a substrate in all cases. A 12 mm wide ITO strip line was made by wet etching at the middle of the substrate. ITO substrates were cleaned by the following method: sonicated in $CHCl_3$; sonicated in acetone; rinsed two times with deionized (DI) water; sonicated in water with 3 vol % of Hellmanex II detergent; rinsed with DI water; and sonicated in DI water and isopropyl alcohol.

OLEDs with structure ITO/PEDOT:PSS(40 nm)/EML(60 nm)/TPBi(20 nm)/LiF(1 nm)/Al(120 nm) or ITO/PEDOT:PSS(40 nm)/EML(60 nm)/BPhen(20 nm)/LiF(1 nm)/Al(120 nm) were prepared. Poly (3,4-ethylenedioxythiophene)-poly (styrenesulfonate) (PEDOT:PSS), 2,2′,2″-(1,3,5-benzinetriyl)-tris(1-phenyl-1-*H*-benzimidazole) (TPBi), and LiF were used as hole-injection, electron transport, and electron-injection layers, respectively. Before deposition of PEDOT:PSS, the ITO glass (50 Ω^2) was blown dry with nitrogen and treated with UV-ozone for 20 min. The ITO layer was covered with PEDOT:PSS (from H.C. Starck, Al4083) using a spin-coater Laurell WS650. The rotation lasted for 1 min with a speed of 2000 rpm. The sample was moved into a glovebox and heated at 150 °C for 30 min. The solution of emitting layer compounds with a concentration of 7 mg/mL in tetrahydrofuran was spin-coated on the PEDOT:PSS layer with 2000 rpm for 40 s and heated at 120 °C for 15 min afterward. The following EMLs were used in different devices: pure push−pull purines; **9b** and bis[2-(4,6-difluorophenyl)pyridinato-C2,N](picolinato)iridium (FIrpic; Ossila) 90:10 wt %; FIrpic/**9b**/4,4′-bis(*N*-carbazolyl)-1,1′-biphenyl (CBP) (10:30:60 wt %); and FIrpic/poly(9-vinylcarbazole) (PVK)/CBP (10:30:60

https://doi.org/10.1021/acsomega.1c06359
ACS Omega 2022, 7, 5242−5253

wt %). Furthermore, the samples were moved from the glovebox to a vacuum chamber, without exposure to air, for thermal evaporation of electron transport TPBi (Sigma Aldrich 806781) or BPhen (Sigma Aldrich 11880), electron-injection LiF (Sigma Aldrich 449903), and electrodes at the pressure 6×10^{-6} Torr. The deposition speed was 1, 0.1, and 5 Å/s for TPBi, LiF, and Al, respectively. The current−voltage characteristics of the OLEDs were measured using a Keithley 2450 SourceMeter. The electroluminescence brightness was measured by Konica Minolta Luminance and Color Meter CS-150. The structure of hole-only device was ITO/MoO_3(10 nm)/compound(60 nm)/MoO_3(10 nm)/Al(100 nm) and the electron-only device was ITO/LiF(1 nm)/compound(60 nm)/ LiF(1 nm)/Al(100 nm). Layer preparation parameters were the same as for OLED.

*General Procedures and Characterization of Products. 9-(5,5,5-Triphenylpentyl)-2,6-dichloro-9H-purine (**2**).* Under an argon atmosphere, diisopropyl azodicarboxylate (DIAD) (7.88 mL, ρ = 1.03 g/cm^3, 40.02 mmol, 1.5 equiv.) was added dropwise to a cooled solution of 2,6-dichloropurine **1** (5.00 g, 26.46 mmol, 1.0 equiv.), 5,5,5-triphenylpentanol[48] (8.79 g, 27.79 mmol, 1.1 equiv.), and Ph_3P (10.21 g, 38.93 mmol, 1.5 equiv.) in absolute THF (40 mL) over 15 min. The reaction mixture was stirred for 1.5 h at 20 °C, controlled by HPLC, then evaporated, the residue was dissolved in EtOH (20 mL), and cooled to −10 °C for 30 min. Formed precipitates were filtered and washed with cold EtOH (2 × 5 mL). The filtrate was evaporated and purified by silica gel column chromatography (DCM/MeCN, gradient 0 → 10%). Yield 8.36 g, 65%. Colorless amorphous solid, R_f = 0.49 (DCM/MeCN = 20/1). HPLC: t_R = 7.63 min. IR (FT-IR): 3081, 2938, 1597, 1558 cm^{-1}. ^{1}H-NMR (300 MHz, $CDCl_3$) δ (ppm): 7.92 (s, 1H, H-C(8)), 7.32−7.14 (m, 15H, H-C(Ph)), 4.15 (t, 2H, ^3J = 7.2 Hz, (−CH_2−)), 2.68−2.55 (m, 2H, (−CH_2−)), 1.91 (quintet, 2H, ^3J = 7.5 Hz, (−CH_2−)), 1.22−1.06 (m, 2H, (−CH_2−)). ^{13}C-NMR (75.5 MHz, $CDCl_3$) δ (ppm): 153.2, 152.9, 151.8, 147.0, 145.7, 130.7, 129.1, 128.0, 126.1, 56.7, 44.5, 39.7, 30.5, 22.9. HRMS (ESI): calcd for [$C_{28}H_{24}Cl_2N_4$ + H^+] 487.1451, found 487.1446.

*2,6-Diazido-9-(5,5,5-triphenylpentyl)-9H-purine (**3**).* NaN_3 (0.20 g, 3.08 mmol, 2.4 equiv.) was added to a solution of alkylated 2,6-dichloropurine **2** (0.62 g, 1.27 mmol, 1.0 equiv.) in acetone (10 mL), stirred for 14 h at 50 °C, covered from the light, controlled by HPLC, evaporated, and suspended in water (30 mL). The formed precipitates were filtered and washed with water (3 × 10 mL) and dried in a vacuum. Yield 0.63 g, 99%. Colorless amorphous solid, R_f = 0.57 (DCM/MeCN = 20/1). HPLC: t_R = 7.73 min. IR (FT-IR): 2154, 2134, 1598, 1577 cm^{-1}. ^{1}H-NMR (300 MHz, $CDCl_3$) δ (ppm): 7.73 (s, 1H, H-C(8)), 7.33−7.12 (m, 15H, H-C(Ph)), 4.07 (t, 2H, ^3J = 7.2 Hz, (−CH_2−)), 2.68−2.55 (m, 2H, (−CH_2−)), 1.88 (quintet, 2H, ^3J = 7.5 Hz, (−CH_2−)), 1.24−1.07 (m, 2H, (−CH_2−)). ^{13}C-NMR (75.5 MHz, $CDCl_3$) δ (ppm): 156.0, 153.9, 153.7, 147.1, 143.5, 129.1, 128.0, 126.1, 121.1, 56.7, 44.0, 39.8, 30.5, 22.9. HRMS (ESI): calcd for [$C_{28}H_{24}N_{10}$ + H^+] 501.2258, found 501.2240.

*6-Azido-9-(5,5,5-triphenylpentyl)-2-(piperidin-1-yl)-9H-purine (**4**).* Piperidine (0.60 mL, ρ = 0.86 g/cm^3, 5.99 mmol, 3.0 equiv.) was added to a solution of compound **3** (1.00 g, 1.99 mmol, 1.0 equiv.) in DMF (20 mL) and stirred for 1 h at 20 °C, covered from the light, controlled by HPLC. The reaction mixture was evaporated and purified by silica gel column chromatography (DCM/MeCN, gradient 0 → 10%). Yield 899 mg, 83%. Light yellow amorphous solid, R_f = 0.38 (DCM/MeCN = 10:1). HPLC: t_R = 9.46 min. IR (FT-IR): 2934, 2852, 2119, 1618, 1567 cm^{-1}. ^{1}H-NMR (300 MHz, $CDCl_3$) δ (ppm): 7.44 (s, 1H, H-C(8)), 7.30−7.06 (m, 15H, H-C(Ph)), 3.96 (t, 2H, ^3J = 7.2 Hz, (−CH_2−)), 3.83−3.72 (m, 4H, 2 × (−CH_2−)), 2.68−2.54 (m, 2H, (−CH_2−)), 1.85 (quintet, 2H, ^3J = 7.4 Hz, (−CH_2−)), 1.74−1.50 (m, 6H, 3 × (−CH_2−)), 1.11 (m, 2H, (−CH_2−)). ^{13}C-NMR (75.5 MHz, $CDCl_3$) δ (ppm): 158.6, 154.8, 152.6, 147.3, 140.5, 129.2, 127.9, 126.0, 117.1, 56.7, 45.4, 42.9, 39.8, 30.5, 25.9, 25.0, 22.8. HRMS (ESI): calcd for [$C_{33}H_{34}N_8$ + H^+] 543.2979, found 543.2986.

*2-Azido-6-(piperidin-1-yl)-9H-purine (**7**).*[49] To a solution of 2,6-dichloropurine (**1**) (3.00 g, 15.90 mmol, 1.0 equiv.) in EtOH (30 mL), a solution of NaN_3 (4.13 g, 63.60 mmol, 4.0 equiv.) in water (15 mL) was added and the reaction mixture was stirred at 100 °C temperature for 30 min, then it was cooled and a colorless precipitate was formed, which was filtered and recrystallized from EtOH (100 mL) to give 2.46 g (w = 75%) of product **6** as a colorless solid. Then, piperidine (4 mL) was added to a suspension of 2,6-diazido-9*H*-purine (**6**) (2.46 g, 12.18 mmol, 1.0 equiv.)[19,50] in water (10 mL) and was stirred at 100 °C temperature for 2.5 h. Then, the reaction mixture was cooled to room temperature and AcOH was added while the pH of the solution reached 7. The mixture was kept in the fridge for 3 h. The precipitate was filtered and washed with cold EtOH (30 mL) and recrystallized from EtOH (75 mL) to give product **7** as a colorless solid. Yield 2.03 g, 52%. mp = 215 °C (decompose). HPLC: t_R = 4.41 min. IR (FT-IR): 3059, 2931, 2819, 2125 (N3), 1603, 1579, 1367 cm^{-1}. ^{1}H-NMR (300 MHz, DMSO-d_6) δ (ppm): 12.76 (brs, 1H, H-N), 7.96 (s, 1H, H-C(8)), 4.27−4.05 (m, 4H, 2 × (−CH_2−)), 1.76−1.53 (m, 6H, 3 × (−CH_2−)). ^{13}C-NMR (75.5 MHz, DMSO-d_6) δ (ppm): 154.8, 153.1, 152.7, 137.6, 116.4, 45.4, 25.6, 24.1.

*2-Azido-9-(5,5,5-triphenylpentyl)-6-(piperidin-1-yl)-9H-purine (**8**).* Under an argon atmosphere, DIAD (0.41 mL, ρ = 1.03 g/cm^3, 2.10 mmol, 1.1 equiv.) was added over 15 min to a cooled solution of 2-azido-6-(piperidin-1-yl)-9*H*-purine (**7**) (460 mg, 1.90 mmol, 1.0 equiv.), 5,5,5-triphenylpentanol (633 mg, 2.00 mmol, 1.05 equiv.), and Ph_3P (550 mg, 2.10 mmol, 1.1 equiv.) in THF (15 mL) and stirred for 12 h at 20 °C, controlled by HPLC, filtered, evaporated, diluted with MeCN (5 mL), and cooled to −10 °C for 30 min. The formed precipitates were filtered and washed with cold MeCN (2 × 3 mL) and dried in a vacuum. Yield 730 mg, 71%. Colorless amorphous solid, R_f = 0.80 (DCM/MeCN = 40:1). HPLC: t_R = 9.18 min. IR (FT-IR): 2938, 2853, 2126, 1588, 1486, 1360, 1339, 1250, 997 cm^{-1}. ^{1}H-NMR (300 MHz, $CDCl_3$) δ (ppm): 7.47 (s, 1H, H-C(8)), 7.32−7.12 (m, 15H, H-C(Ph)), 4.44−4.04 (m, 4H, 2 × (−CH_2−)), 3.99 (t, 2H, ^3J = 7.4 Hz, (−CH_2−)), 2.64−2.54 (m, 2H, (−CH_2−)), 1.84 (quintet, 2H, ^3J = 7.4 Hz, (−CH_2−)), 1.83−1.64 (m, 6H, 3 × (−CH_2−)), 1.20−1.07 (m, 2H, (−CH_2−)). ^{13}C-NMR (75.5 MHz, $CDCl_3$) δ (ppm): 156.1, 153.9, 152.5, 147.2, 137.6, 129.2, 128.0, 126.0, 117.5, 56.7, 46.3 (assigned from the HSQC spectrum at 50 °C temperature), 43.5, 39.9, 30.7, 26.2, 24.9, 23.0. HRMS (ESI): calcd for [$C_{33}H_{34}N_8$ + H^+] 543.2979, found 543.2980.

*Synthesis of 2-(Piperidin-1-yl)-6-triazolyl-9-alkylpurines **5**. 6-(4-(4-Methoxyphenyl)-1H-1,2,3-triazol-1-yl)-9-(5,5,5-triphenylpentyl)-2-(piperidin-1-yl)-9H-purine (**5b**).* 10% AcOH solution in water (1.0 mL), sodium ascorbate (85 mg, 0.43 mmol, 0.9 equiv.), and $CuSO_4 \cdot 5H_2O$ (51 mg, 0.20 mmol, 44 mol %) were added to a solution of compound **4** (250 mg, 0.46 mmol, 1.0 equiv.) and 4-methoxyphenylacetylene (0.15 mL, ρ = 1.02 g/cm^3, 1.16 mmol, 2.5 equiv.) in THF (10 mL) and stirred for 4 h at 20 °C. The reaction mixture was evaporated, the

https://doi.org/10.1021/acsomega.1c06359
ACS Omega 2022, 7, 5242−5253

residue was dissolved in DCM (20 mL), and washed with NaHS solution (3 × 5 mL). The DCM layer was dried over anhydrous Na_2SO_4, filtered, evaporated, and purified by silica gel column chromatography (DCM/MeCN = 5/1). Yield 240 mg, 77%. Yellow amorphous solid, R_f = 0.76 (DCM/MeCN = 5:1). HPLC: t_R = 8.75 min, purity 97%. IR (FT-IR): 2933, 2851, 1718, 1628, 1565 cm^{-1}. ^{1}H-NMR (300 MHz, $CDCl_3$) δ (ppm): 9.00 (s, 1H, H-C(triazole)), 7.95 (d, 2H, ^3J = 8.6 Hz, Ar), 7.68 (s, 1H, H-C(8)), 7.24−7.09 (m, 15H, Ar), 7.01 (d, 2H, ^3J = 8.6 Hz, Ar), 4.05 (t, 2H, ^3J = 7.1 Hz, (−CH_2−)), 3.92−3.80 (m, 7H, 2 × (−CH_2−), (−CH_3)), 2.70−2.58 (m, 2H, (−CH_2−)), 1.90 (quintet, 2H, ^3J = 7.1 Hz, (−CH_2−)), 1.76−1.56 (m, 6H, 3 × (−CH_2−)), 1.23−1.08 (m, 2H, (−CH_2−)). ^{13}C-NMR (75.5 MHz, $CDCl_3$) δ (ppm): 160.0, 158.4, 156.9, 147.5, 147.2, 145.1, 142.5, 129.2, 128.0, 127.7, 126.1, 123.1, 118.5, 115.5, 114.4, 56.7, 55.5, 45.6, 43.1, 39.8, 30.5, 25.9, 24.9, 22.8. HRMS (ESI): calcd for [$C_{42}H_{42}N_8O$ + H^+] 675.3554, found 675.3545.

*General Synthetic Procedure for 1,3-Dipolar Cycloaddition Reaction for 5a, 5c, 5d, and **9a−d**.* DIPEA (104 μL, ρ = 0.74 g/cm^3, 0.61 mmol, 1.1 equiv.), AcOH (37 μL, ρ = 1.05 g/cm^3, 0.61 mmol, 1.1 equiv.), and CuI (21 mg, 0.11 mmol, 0.2 equiv.) were added to a solution of 2-amino-6-azidopurine **4** or 6-amino-2-azidopurine **8** (300 mg, 0.55 mmol, 1.0 equiv.) and alkyne (1.5 equiv.) in DCM (9 mL) and stirred for 14−264 h at 20 °C, covered from the light, and controlled by HPLC. The reaction mixture was poured into the water (20 mL) and extracted with DCM (3 × 10 mL). Organic layers were combined and washed with diluted NaHS solution (10 mL), filtered through Celite, separated, and washed with brine (10 mL), dried over anhydrous Na_2SO_4, filtered, evaporated, and purified by silica gel column chromatography (DCM/MeCN, gradient 0 → 25%).

*6-(4-Phenyl-1H-1,2,3-triazol-1-yl)-9-(5,5,5-triphenylpentyl)-2-(piperidin-1-yl)-9H-purine (**5a**).* Reaction time: 14 h. Yield 282 mg, 79%. Light yellow amorphous solid, R_f = 0.23 (DCM/MeCN = 10:1). HPLC: t_R = 8.49 min. IR (FT-IR): 3055, 2932, 2851, 1628, 1565, 1533, 1446, 1009 cm^{-1}. ^{1}H-NMR (300 MHz, $CDCl_3$) δ (ppm): 9.07 (s, 1H, H-C(triazole)), 7.99 (d, 2H, ^3J = 7.3 Hz, H-C(Ph)), 7.80 (s, 1H, H-C(8)), 7.47 (t, 2H, ^3J = 7.3 Hz, H-C(Ph)), 7.37 (t, 1H, ^3J = 7.3 Hz, H-C(Ph)), 7.25−7.08 (m, 15H, H-C(Ph)), 4.07 (t, 2H, ^3J = 7.0 Hz, (−CH_2−)), 3.92−3.82 (m, 4H, 2 × (−CH_2−)), 2.70−2.59 (m, 2H, (−CH_2−)), 1.91 (quintet, 2H, ^3J = 7.0 Hz, (−CH_2−)), 1.76−1.56 (m, 6H, 3 × (−CH_2−)), 1.24−1.08 (m, 2H, (−CH_2−)). ^{13}C-NMR (75.5 MHz, $CDCl_3$) δ (ppm): 158.3, 156.7, 147.5, 147.1, 144.9, 142.6, 130.3, 129.1, 128.9, 128.4, 127.9, 126.2, 126.0, 119.2, 115.2, 56.6, 45.5, 43.0, 39.7, 30.4, 25.8, 24.8, 22.7. HRMS (ESI): calcd for [$C_{41}H_{40}N_8$ + H^+] 645.3449, found 645.3443.

*9-(5,5,5-Triphenylpentyl)-6-(4-(4-(N,N-dimethylamino)-phenyl)-1H-1,2,3-triazol-1-yl)-2-(piperidin-1-yl)-9H-purine (**5c**).* Reaction time: 64 h. Yield 249 mg, 66%. Yellow amorphous solid, R_f = 0.26 (DCM/MeCN = 10:1). HPLC: t_R = 7.59 min. IR (FT-IR): 2932, 2856, 1622, 1561, 1561, 1538, 1491, 1445, 1410, 1359, 1020 cm^{-1}. ^{1}H-NMR (300 MHz, $CDCl_3$) δ (ppm): 8.95 (s, 1H, H-C(triazole)), 7.88 (d, 2H, ^3J = 8.7 Hz, H-C(Ar)), 7.67 (s, 1H, H-C(8)), 7.26−7.10 (m, 15H, H-C(Ph)), 6.82 (d, 2H, ^3J = 8.7 Hz, H-C(Ar)), 4.05 (t, 2H, ^3J = 7.1 Hz, (−CH_2−)), 3.92−3.82 (m, 4H, 2 × (−CH_2−)), 3.01 (s, 6H, (Me)$_2$N−), 2.69−2.60 (m, 2H, (−CH_2−)), 1.90 (quintet, 2H, ^3J = 7.1 Hz, (−CH_2−)), 1.74−1.58 (m, 6H, 3 × (−CH_2−)), 1.24−1.08 (m, 2H, (−CH_2−)). ^{13}C-NMR (75.5 MHz, $CDCl_3$) δ (ppm): 158.4, 156.8, 150.6, 148.0, 147.2, 145.2, 142.3, 129.2, 127.9, 127.3, 126.0, 118.7, 117.6, 115.5, 112.6, 56.7, 45.6, 43.0, 40.7, 39.8, 30.5, 25.9, 24.9, 22.8. HRMS (ESI): calcd for [$C_{43}H_{45}N_9$ + H^+] 688.3871, found 688.3888.

*6-(4-(4-Cyanophenyl)-1H-1,2,3-triazol-1-yl)-9-(5,5,5-triphenylpentyl)-2-(piperidin-1-yl)-9H-purine (**5d**).* Reaction time: 14 h. Silica gel column chromatography (DCM/MeCN, gradient 0 → 10%). Yield 298 mg, 81%. Light yellow amorphous solid, R_f = 0.40 (DCM/MeCN = 10:1). HPLC: t_R = 8.15 min. IR (FT-IR): 2934, 2852, 2225, 1630, 1564, 1534, 1491, 1446, 1412, 1232, 1010 cm^{-1}. ^{1}H-NMR (300 MHz, $CDCl_3$) δ (ppm): 9.21 (s, 1H, H-C(triazole)), 8.13 (d, 2H, ^3J = 8.4 Hz, H-C(Ar)), 7.76 (d, 2H, ^3J = 8.4 Hz, H-C(Ar)), 7.71 (s, 1H, H-C(8)), 7.24−7.10 (m, 15H, H-C(Ph)), 4.07 (t, 2H, ^3J = 7.2 Hz, (−CH_2−)), 3.92−3.83 (m, 4H, 2 × (−CH_2−)), 2.69−2.59 (m, 2H, (−CH_2−)), 1.91 (quintet, 2H, ^3J = 7.2 Hz, (−CH_2−)), 1.74−1.58 (m, 6H, 3 × (−CH_2−)), 1.22−1.10 (m, 2H, (−CH_2−)). ^{13}C-NMR (75.5 MHz, $CDCl_3$) δ (ppm): 158.4, 157.0, 147.2, 145.8, 144.6, 142.8, 134.8, 132.8, 129.2, 128.0, 126.7, 126.1, 120.7, 118.9, 115.4, 111.9, 56.7, 45.6, 43.2, 39.8, 30.4, 25.9, 24.9, 22.8. HRMS (ESI): calcd for [$C_{42}H_{39}N_9$ + H^+] 670.3401, found 670.3406.

*Synthesis of 6-(Piperidin-1-yl)-2-triazolyl-9-alkylpurines **9**. 2-(4-Phenyl-1H-1,2,3-triazol-1-yl)-6-(piperidin-1-yl)-9-(5,5,5-triphenylpentyl)-9H-purine (**9a**).* Reaction time: 72 h. Yield 314 mg, 88%. Colorless amorphous solid, R_f = 0.27 (DCM/MeCN = 20:1). HPLC: t_R = 9.42 min. IR (FT-IR): 3055, 2934, 2853, 1595, 1492, 1437, 1251, 1017 cm^{-1}. ^{1}H-NMR (300 MHz, $CDCl_3$) δ (ppm): 8.64 (s, 1H, H-C(triazole)), 7.95 (d, 2H, ^3J = 7.2 Hz, H-C(Ph)), 7.63 (s, 1H, H-C(8)), 7.46 (t, 2H, ^3J = 7.2 Hz, H-C(Ph)), 7.36 (t, 1H, ^3J = 7.2 Hz, H-C(Ph)), 7.24−7.06 (m, 15H, H-C(Ph)), 4.42−4.24 (m, 4H, 2 × (−CH_2−)), 4.15 (t, 2H, ^3J = 7.2 Hz, (−CH_2−)), 2.67−2.58 (m, 2H, (−CH_2−)), 1.92 (quintet, 2H, ^3J = 7.2 Hz, (−CH_2−)), 1.82−1.72 (m, 6H, 3 × (−CH_2−)), 1.28−1.15 (m, 2H, (−CH_2−)). ^{13}C-NMR (75.5 MHz, $CDCl_3$) δ (ppm): 153.9, 151.7, 149.3, 147.4, 147.2, 138.7, 130.7, 129.2, 128.9, 128.3, 128.0, 126.2, 126.0, 119.0, 118.8, 56.7, 46.7 (assigned from the HSQC spectrum at 50 °C temperature), 43.7, 39.9, 30.8, 26.3, 24.8, 23.0. HRMS (ESI): calcd for [$C_{41}H_{40}N_8$ + H^+] 645.3449, found 645.3439.

*2-(4-(4-Methoxyphenyl)-1H-1,2,3-triazol-1-yl)-6-(piperidin-1-yl)-9-(5,5,5-triphenylpentyl)-9H-purine (**9b**).* Reaction time: 240 h. Yield 274 mg, 73%. Colorless amorphous solid, R_f = 0.23 (DCM/MeCN = 20:1). HPLC: t_R = 8.57 min. IR (FT-IR): 3053, 2934, 2853, 1594, 1567, 1492, 1445, 1249, 1020 cm^{-1}. ^{1}H-NMR (300 MHz, $CDCl_3$) δ (ppm): 8.56 (s, 1H, H-C(triazole)), 7.87 (d, 2H, ^3J = 8.8 Hz, H-C(Ar)), 7.63 (s, 1H, H-C(8)), 7.25−7.08 (m, 15H, H-C(Ph)), 6.99 (d, 2H, ^3J = 8.8 Hz, H-C(Ar)), 4.45−4.20 (m, 4H, 2 × (−CH_2−)), 4.15 (t, 2H, ^3J = 7.2 Hz, (−CH_2−)), 3.87 (s, 3H, H_3C-O), 2.66−2.58 (m, 2H, (−CH_2−)), 1.92 (quintet, 2H, ^3J = 7.2 Hz, (−CH_2−)), 1.82−1.71 (m, 6H, 3 × (−CH_2−)), 1.29−1.14 (m, 2H, (−CH_2−)). ^{13}C-NMR (75.5 MHz, $CDCl_3$) δ (ppm): 159.8, 153.9, 151.7, 149.3, 147.2 (2C) (assigned from the HMBC spectrum), 138.7, 129.2, 127.9, 127.5, 126.0, 123.4, 119.0, 117.9, 114.3, 56.7, 55.5, 46.7 (assigned from the HSQC spectrum at 50 °C temperature), 43.7, 39.9, 30.7, 26.3, 24.8, 23.1. HRMS (ESI): calcd for [$C_{42}H_{42}N_8O$ + H^+] 675.3554, found 675.3566.

*9-(5,5,5-Triphenylpentyl)-2-(4-(4-(N,N-dimethylamino)-phenyl)-1H-1,2,3-triazol-1-yl)-6-(piperidin-1-yl)-9H-purine (**9c**).* Reaction time: 264 h. Yield 320 mg, 85%. Beige amorphous solid, R_f = 0.68 (DCM/MeCN = 10:1). HPLC: t_R = 7.55 min. IR (FT-IR): 2934, 2853, 1594, 1571, 1492, 1443, 1356, 1251, 1024 cm^{-1}. ^{1}H-NMR (300 MHz, $CDCl_3$) δ (ppm): 8.51 (s, 1H, H-C(triazole)), 7.81 (d, 2H, ^3J = 8.7 Hz, H-C(Ar)), 7.60 (s, 1H, H-

https://doi.org/10.1021/acsomega.1c06359
ACS Omega 2022, 7, 5242−5253

C(8)), 7.24−7.09 (m, 15H, H-C(Ph)), 6.82 (d, 2H, ^3J = 8.7 Hz, H-C(Ar)), 4.42−4.24 (m, 4H, 2 × (−CH_2−)), 4.14 (t, 2H, ^3J = 7.3 Hz, (−CH_2−)), 3.01 (s, 6H, (($Me)_2$N−)), 2.66−2.57 (m, 2H, (−CH_2−)), 1.92 (quintet, 2H, ^3J = 7.3 Hz, (−CH_2−)), 1.81−1.71 (m, 6H, 3 × (−CH_2−)), 1.28−1.14 (m, 2H, (−CH_2−)). ^{13}C-NMR (75.5 MHz, $CDCl_3$) δ (ppm): 153.9, 151.7, 150.6, 149.4, 147.8, 147.2, 138.6, 129.2, 127.9, 127.1, 125.9, 119.0, 118.9, 117.2, 112.6, 56.7, 46.6 (assigned from the HSQC spectrum at 50 °C temperature), 43.7, 40.6, 39.9, 30.7, 26.3, 24.8, 23.1. HRMS (ESI): calcd for [$C_{43}H_{45}N_9$ + H^+] 688.3871, found 688.3878.

*2-(4-(4-Cyanophenyl)-1H-1,2,3-triazol-1-yl)-9-(5,5,5-triphenylpentyl)-6-(piperidin-1-yl)-9H-purine (**9d**).* Reaction time: 144 h. Yield 317 mg, 86%. Colorless amorphous solid, R_f = 0.85 (DCM/MeCN = 10:1). HPLC: t_R = 8.41 min. IR (FT-IR): 2937, 2856, 2226, 1597, 1571, 1493, 1445, 1251, 1025 cm^{-1}. ^{1}H-NMR (300 MHz, $CDCl_3$) δ (ppm): 8.73 (s, 1H, H-C(triazole)), 8.05 (d, 2H, ^3J = 8.4 Hz, H-C(Ar)), 7.73 (d, 2H, ^3J = 8.4 Hz, H-C(Ar)), 7.63 (s, 1H, H-C(8)), 7.24−7.08 (m, 15H, H-C(Ph)), 4.44−4.24 (m, 4H, 2 × (−CH_2−)), 4.15 (t, 2H, ^3J = 7.3 Hz, (−CH_2−)), 2.67−2.58 (m, 2H, (−CH_2−)), 1.92 (quintet, 2H, ^3J = 7.3 Hz, (−CH_2−)), 1.83−1.70 (m, 6H, 3 × (−CH_2−)), 1.27−1.12 (m, 2H, (−CH_2−)). ^{13}C-NMR (75.5 MHz, $CDCl_3$) δ (ppm): 153.9, 151.6, 149.1, 147.2, 145.6, 138.9, 135.1, 132.8, 129.2, 128.0, 126.5, 126.1, 120.0, 119.3, 119.0, 111.7, 56.7, 46.6 (assigned from the HSQC spectrum at 50 °C temperature), 43.7, 39.9, 30.8, 26.3, 24.8, 23.1. HRMS (ESI): calcd for [$C_{42}H_{39}N_9$ + H^+] 670.3401, found 670.3383.

■ ASSOCIATED CONTENT

Supporting Information

The Supporting Information is available free of charge at https://pubs.acs.org/doi/10.1021/acsomega.1c06359.

Supporting Information file contains figures of thermogravimetric analysis of compounds **9a** and **9b**, emission lifetime measurements for compounds **5a−d** and **9a−d**, fluorescence and phosphorescence spectra of **5b−c** and **9b−c** in the 2-MeTHF matrix at 77 K, current density−voltage dependencies for purine-only and purine host-FIrpic OLEDs, calculated dipole momentum values of the compounds, radiative and nonradiative decay rates of the compounds, and NMR spectra of compounds **2**, **3**, **4**, **7**, **8**, **5a−d**, and **9a−d** (PDF)

■ AUTHOR INFORMATION

Corresponding Authors

Irina Novosjolova − *Faculty of Materials Science and Applied Chemistry, Riga Technical University, LV-1048 Riga, Latvia;* orcid.org/0000-0002-9607-2222; Email: irina.novosjolova@rtu.lv

Kaspars Traskovskis − *Faculty of Materials Science and Applied Chemistry, Riga Technical University, LV-1048 Riga, Latvia;* orcid.org/0000-0003-1416-7533; Email: kaspars.traskovskis@rtu.lv

Māris Turks − *Faculty of Materials Science and Applied Chemistry, Riga Technical University, LV-1048 Riga, Latvia;* orcid.org/0000-0001-5227-0369; Email: maris.turks@rtu.lv

Authors

Armands Sebris − *Faculty of Materials Science and Applied Chemistry, Riga Technical University, LV-1048 Riga, Latvia*

Valdis Kokars − *Faculty of Materials Science and Applied Chemistry, Riga Technical University, LV-1048 Riga, Latvia*

Natalija Tetervenoka − *Institute of Solid State Physics, University of Latvia, LV-1063 Riga, Latvia*

Aivars Vembris − *Institute of Solid State Physics, University of Latvia, LV-1063 Riga, Latvia*

Complete contact information is available at: https://pubs.acs.org/10.1021/acsomega.1c06359

Notes

The authors declare no competing financial interest.

■ ACKNOWLEDGMENTS

This work is supported by the ERDF 1.1.1.1. activity project No. 1.1.1.1/16/A/131. The authors thank Dr. sc. ing. Jānis Zicāns and Dr. sc. ing. Remo Merijs Meri for DSC analyses.

■ REFERENCES

(1) Gomez, E. F.; Venkatraman, V.; Grote, J. G.; Steckl, A. J. DNA Bases Thymine and Adenine in Bio-Organic Light Emitting Diodes. *Sci. Rep.* **2014**, *4*, No. 7105.

(2) Gomez, E. F.; Venkatraman, V.; Grote, J. G.; Steckl, A. J. Exploring the Potential of Nucleic Acid Bases in Organic Light Emitting Diodes. *Adv. Mater.* **2015**, *27*, 7552−7562.

(3) Cho, M. J.; Lee, U. R.; Kim, Y. S.; Shin, J.; Kim, Y. M.; Park, Y. W.; Ju, B.-K.; Jin, J.-I.; Choi, D. H. Organic Soluble Deoxyribonucleic Acid (DNA) Bearing Carbazole Moieties and Its Blend with Phosphorescent Ir (III) Complexes. *J. Polym. Sci., Part A: Polym. Chem.* **2010**, *48*, 1913−1918.

(4) Irimia-Vladu, M.; Troshin, P. A.; Reisinger, M.; Shmygleva, L.; Kanbur, Y.; Schwabegger, G.; Bodea, M.; Schwödiauer, R.; Mumyatov, A.; Fergus, J. W.; et al. Biocompatible and Biodegradable Materials for Organic Field-Effect Transistors. *Adv. Funct. Mater.* **2010**, *20*, 4069−4076.

(5) Kim, Y. S.; Jung, K. H.; Lee, U. R.; Kim, K. H.; Hoang, M. H.; Jin, J.-I.; Choi, D. H. High-Mobility Bio-Organic Field Effect Transistors with Photoreactive DNAs as Gate Insulators. *Appl. Phys. Lett.* **2010**, *96*, No. 103307.

(6) Butler, R. S.; Myers, A. K.; Bellarmine, P.; Abboud, K. A.; Castellano, R. K. Highly Fluorescent Donor-Acceptor Purines. *J. Mater. Chem.* **2007**, *17*, 1863−1865.

(7) Butler, R. S.; Cohn, P.; Tenzel, P.; Abboud, K. A.; Castellano, R. K. Synthesis, Photophysical Behavior, and Electronic Structure of Push-Pull Purines. *J. Am. Chem. Soc.* **2009**, *131*, 623−633.

(8) Vabre, R.; Legraverend, M.; Piguel, S. Synthesis and Evaluation of Spectroscopic Properties of Newly Synthesized Push-Pull 6-Amino-8-styryl Purines. *Dyes Pigm.* **2014**, *105*, 145−151.

(9) Collier, G. S.; Brown, L. A.; Boone, E. S.; Kaushal, M.; Ericson, M. N.; Walter, M. G.; Long, B. K.; Kilbey, S. M. Linking Design and Properties of Purine-Based Donor-Acceptor Chromophores as Optoelectronic Materials. *J. Mater. Chem. C* **2017**, *5*, 6891−6898.

(10) Zucolotto Cocca, L. H.; Abegaõ, L. M. G.; Sciuti, L. F.; Vabre, R.; De Paula Siqueira, J.; Kamada, K.; Mendonca, C. R.; Piguel, S.; De Boni, L. Two-Photon Emissive Dyes Based on Push-Pull Purines Derivatives: Toward the Development of New Photoluminescence Bioprobes. *J. Phys. Chem. C* **2020**, *124*, 12617−12627.

(11) Pelosi, A. G.; Zucolotto Cocca, L. H.; Abegão, L. M. G.; Sciuti, L. F.; Piguel, S.; De Boni, L.; Mendonça, C. R. Influence of Electron-Withdrawing Groups in Two-Photon Absorption of Imidazopyridines Derivatives. *Dyes Pigm.* **2022**, *198*, No. 109972.

(12) Jacquemin, D.; Escudero, D. The Short Device Lifetimes of Blue PhOLEDs: Insights into the Photostability of Blue Ir(III) Complexes. *Chem. Sci.* **2017**, *8*, 7844−7850.

(13) Yang, Y.; Cohn, P.; Eom, S.-H.; Abboud, K. A.; Castellano, R. K.; Xue, J. Ultraviolet-Violet Electroluminescence from Highly Fluorescent Purines. *J. Mater. Chem. C* **2013**, *1*, 2867−2874.

(14) Yang, Y.; Cohn, P.; Dyer, A. L.; Eom, S.-H.; Reynolds, J. R.; Castellano, R. K.; Xue, J. Blue-Violet Electroluminescence from a Highly Fluorescent Purine. *Chem. Mater.* **2010**, *22*, 3580−3582.
(15) Wang, Z.; Yao, J.; Zhan, L.; Gong, S.; Ma, D.; Yang, C. Purine-Based Thermally Activated Delayed Fluorescence Emitters for Efficient Organic Light-Emitting Diodes. *Dyes Pigm.* **2020**, *180*, No. 108437.
(16) Sebris, A.; Traskovskis, K.; Novosjolova, I.; Turks, M. Synthesis and Photophysical Properties of Purine-Phenoxazine and Purine-Phenothiazine Conjugates. *Key Eng. Mater.* **2021**, *903*, 155−161.
(17) Traskovskis, K.; Sebris, A.; Novosjolova, I.; Turks, M.; Guzauskas, M.; Volyniuk, D.; Bezvikonnyi, O.; Grazulevicius, J. V.; Mishnev, A.; Grzibovskis, R.; et al. All-Organic Fast Intersystem Crossing Assisted Exciplexes Exhibiting Sub-Microsecond Thermally Activated Delayed Fluorescence. *J. Mater. Chem. C* **2021**, *9*, 4532−4543.
(18) Novosjolova, I.; Bizdēna, Ē.; Turks, M. Synthesis and Applications of Azolylpurine and Azolylpurine Nucleoside Derivatives. *Eur. J. Org. Chem.* **2015**, *2015*, 3629−3649.
(19) Kovaļovs, A.; Novosjolova, I.; Bizdēna, Ē.; Bižāne, I.; Skardziute, L.; Kazlauskas, K.; Jursenas, S.; Turks, M. 1,2,3-Triazoles as Leaving Groups in Purine Chemistry: A Three-Step Synthesis of N6-Substituted-2-triazolyl-adenine Nucleosides and Photophysical Properties Thereof. *Tetrahedron Lett.* **2013**, *54*, 850−853.
(20) Ozols, K.; Cīrule, D.; Novosjolova, I.; Stepanovs, D.; Liepinsh, E.; Bizdēna, Ē.; Turks, M. Development of N6-Methyl-2-(1,2,3-triazol-1-yl)-2′-deoxyadenosine as a Novel Fluorophore and Its Application in Nucleotide Synthesis. *Tetrahedron Lett.* **2016**, *57*, 1174−1178.
(21) Cīrule, D.; Ozols, K.; Platnieks, O.; Bizdēna, Ē.; Māliņa, I.; Turks, M. Synthesis of Purine Nucleoside-Amino Acid Conjugates and Their Photophysical Properties. *Tetrahedron* **2016**, *72*, 4177−4185.
(22) Šišuļins, A.; Bucevičius, J.; Tseng, Y.-T.; Novosjolova, I.; Traskovskis, K.; Bizdēna, Ē.; Chang, H.-T.; Tumkevičius, S.; Turks, M. Synthesis and Fluorescent Properties of N(9)-Alkylated 2-Amino-6-triazolylpurines and 7-Deazapurines. *Beilstein J. Org. Chem.* **2019**, *15*, 474−489.
(23) Sebris, A.; Traskovskis, K.; Novosjolova, I.; Turks, M. Synthesis and Photophysical Properties of 2-Azolyl-6-piperidinylpurines. *Chem. Heterocycl. Compd.* **2021**, *57*, 560−567.
(24) Kim, M. K.; Kwon, J.; Kwon, T.-H.; Hong, J.-I. A Bipolar Host Containing 1, 2, 3-Triazole for Realizing Highly Efficient Phosphorescent Organic Light-Emitting Diodes. *New J. Chem.* **2010**, *34*, 1317−1322.
(25) Traskovskis, K.; Ruduss, A.; Kokars, V.; Mihailovs, I.; Lesina, N.; Vembris, A. Thiphenylmethane Based Structural Fragments as Building Blocks Towards Solution-Processable Heteroleptic Iridium(III) Complexes for OLED Use. *New J. Chem.* **2019**, *43*, 37−47.
(26) Toyota, A.; Katagiri, N.; Kaneko, C. Mitsunobu Reactions for the Synthesis of Carbocyclic Analogues of Nucleosides: Examination of the Regioselectivity. *Synth. Commun.* **1993**, *23*, 1295−1305.
(27) Manvar, A.; Shah, A. Diversity Oriented Efficient Access of Trisubstituted Purines via Sequential Regioselective Mitsunobu Coupling and S_NAr Based C6 Functionalizations. *Tetrahedron* **2013**, *69*, 680−691.
(28) Bucevicius, J.; Turks, M.; Tumkevicius, S. Easy Access to Isomeric 7-Deazapurine−1,2,3-Triazole Conjugates via S_NAr and CuAAC Reactions of 2,6-Diazido-7-deazapurines. *Synlett* **2018**, *29*, 525−529.
(29) Tsai, M.-H.; Hong, Y.-H.; Chang, C.-H.; Su, H.-C.; Wu, C.-C.; Matoliukstyte, A.; Simokaitiene, J.; Grigalevicius, S.; Grazulevicius, J. V.; Hsu, C.-P. 3-(9-Carbazolyl)carbazoles and 3,6-Di(9-carbazolyl)-carbazoles as Effective Host Materials for Efficient Blue Organic Electrophosphorescence. *Adv. Mater.* **2007**, *19*, 862−866.
(30) Karle, J.; Huang, L. The Glue That Holds Crystals Together: A Review. *J. Mol. Struct.* **2003**, *647*, 9−16.
(31) Wang, X.-J.; You, J.-Z. Study on the Molecular Structure and Thermal Stability of Purine Nucleoside Analogs. *J. Anal. Appl. Pyrolysis* **2015**, *111*, 1−14.
(32) Boelke, A.; Vlasenko, Y. A.; Yusubov, M. S.; Nachtsheim, B. J.; Postnikov, P. S. Thermal Stability of N-Heterocycle-Stabilized Iodanes − a Systematic Investigation. *Beilstein J. Org. Chem.* **2019**, *15*, 2311−2318.
(33) Crespo-Hernández, C. E.; Martínez-Fernández, L.; Rauer, C.; Reichardt, C.; Mai, S.; Pollum, M.; Marquetand, P.; González, L.; Corral, I. Electronic and Structural Elements That Regulate the Excited-State Dynamics in Purine Nucleobase Derivatives. *J. Am. Chem. Soc.* **2015**, *137*, 4368−4381.
(34) Traskovskis, K.; Sebris, A.; Novosjolova, I.; Turks, M.; Guzauskas, M.; Volyniuk, D.; Bezvikonnyi, O.; Grazulevicius, J. V.; Mishnev, A.; Grzibovskis, R.; et al. All-Organic Fast Intersystem Crossing Assisted Exciplexes Exhibiting Sub-microsecond Thermally Activated Delayed Fluorescence. *J. Mater. Chem. C* **2021**, *9*, 4532−4543.
(35) Taft, R. W.; Kamlet, M. J. The Solvatochromic Comparison Method. 2. The Alpha-Scale of Solvent Hydrogen-Bond Donor (HBD) Acidities. *J. Am. Chem. Soc.* **1976**, *98*, 2886−2894.
(36) Reichardt, C. Solvatochromic Dyes as Solvent Polarity Indicators. *Chem. Rev.* **1994**, *94*, 2319−2358.
(37) Lee, J.; Aizawa, N.; Numata, M.; Adachi, C.; Yasuda, T. Versatile Molecular Functionalization for Inhibiting Concentration Quenching of Thermally Activated Delayed Fluorescence. *Adv. Mater.* **2017**, *29*, No. 1604856.
(38) Royakkers, J.; Minotto, A.; Congrave, D. G.; Zeng, W.; Hassan, A.; Leventis, A.; Cacialli, F.; Bronstein, H. Suppressing Solid-State Quenching in Red-Emitting Conjugated Polymers. *Chem. Mater.* **2020**, *32*, 10140−10145.
(39) Reineke, S.; Baldo, M. A. Recent Progress in the Understanding of Exciton Dynamics within Phosphorescent OLEDs. *Phys. Status Solidi A* **2012**, *209*, 2341−2353.
(40) Wiesmann, C.; Bergenek, K.; Linder, N.; Schwarz, U. T. Photonic Crystal LEDs - Designing Light Extraction. *Laser Photonics Rev.* **2009**, *3*, 262−286.
(41) Zhang, T.; He, S. J.; Wang, D. K.; Jiang, N.; Lu, Z. H. A Multi-Zoned White Organic Light-Emitting Diode with High CRI and Low Color Temperature. *Sci. Rep.* **2016**, *6*, No. 20517.
(42) Lin, M. S.; Yang, S. J.; Chang, H. W.; Huang, Y. H.; Tsai, Y. T.; Wu, C. C.; Chou, S. H.; Mondal, E.; Wong, K. T. Incorporation of a CN Group into MCP: A New Bipolar Host Material for Highly Efficient Blue and White Electrophosphorescent Devices. *J. Mater. Chem.* **2012**, *22*, 16114−16120.
(43) Novosjolova, I.; Bizdēna, Ē.; Belyakov, S.; Turks, M. The Synthesis and X-Ray Studies of 6-Pyrrolidinyl-2-triazolyl Purine Arabinonucleoside. *Mater. Sci. Appl. Chem.* **2013**, *28*, 39−44.
(44) Latvels, J.; Grzibovskis, R.; Pudzs, K.; Vembris, A.; Blumberga, D. Photoelectrical Properties of Indandione Fragment Containing Azobenzene Compounds. *Org. Photonics VI* **2014**, *9137*, No. 91371G.
(45) Neese, F. The ORCA Program System. *Wiley Interdiscip. Rev. Comput. Mol. Sci.* **2012**, *2*, 73−78.
(46) Hanwell, M. D.; Curtis, D. E.; Lonie, D. C.; Vandermeerschd, T.; Zurek, E.; Hutchison, G. R. Avogadro: An Advanced Semantic Chemical Editor, Visualization, and Analysis Platform. *J. Cheminform.* **2012**, *4*, No. 17.
(47) Krishnan, R.; Binkley, J. S.; Seeger, R.; Pople, J. A. Self-consistent Molecular Orbital Methods. XX. A Basis Set for Correlated Wave Functions. *J. Chem. Phys.* **1980**, *72*, 650−654.
(48) Jensen, F. R.; Bedard, R. L. Cleavage of Tetrahydrofuran by Triphenylmethylmagnesium Bromide. *J. Org. Chem.* **1959**, *24*, 874−875.
(49) Smirnova, N. B.; Postovskii, I. Y. Some Purine Azides. *Zh. Vsesoyuznogo Khim. Obs. im. D.I. Mendeleeva* **1964**, *9*, 711−712.
(50) Temple, C.; Kussner, C. L.; Montgomery, J. A. Studies on the Azidoazomethine-Tetrazole Equilibrium. V. 2- and 6-Azidopurines 1. *J. Org. Chem.* **1966**, *31*, 2210−2215.

https://doi.org/10.1021/acsomega.1c06359
ACS Omega 2022, 7, 5242−5253